



# Three-Dimensional Stochastic Train-Bridge Coupling Dynamics Under Aftershocks

Ping Xiang<sup>1,2,3,4,5,6</sup> · Peidong Guo<sup>1</sup> · Wangbao Zhou<sup>1,2</sup> · Xiang Liu<sup>1</sup> · Lizhong Jiang<sup>1,2</sup> · Zhiwu Yu<sup>1,2</sup> · Jian Yu<sup>1</sup>

Received: 21 January 2022 / Revised: 3 October 2022 / Accepted: 8 November 2022 / Published online: 18 June 2023  
© The Author(s), under exclusive licence to the Iran University of Science and Technology 2023

## Abstract

The deformation of the track on bridge after the earthquake mainly includes bridge creep and seismic-induced deformation, which poses a serious threat to the running safety of trains. In order to study the influence of the comprehensive deformation on the train-bridge system, a three-dimensional model of train-bridge coupling analysis was established. New point estimation method was used to solve the stochastic problem of initial track irregularity, aiming to study the changes of system motion under different parameters including deformation degrees and train speed. Results show that system motion increases with the increase of track parameters, and the earthquake intensity has the greatest influence on the train the motion, which reaches the peak in 0.4 g. The train speed has the greatest influences on the bridge when the train speed reaches the peak value of 400 km/h, while the impact of bridge creep is the smallest. Conclusion was obtained that the results of random analysis are of more general significance, and that in the vehicle-bridge system considering comprehensive track deformation after earthquake, the damage effect of track deformation induced by earthquake intensity is mainly considered for train, and the impact of train speed shall be mainly considered in bridge design.

**Keywords** Structure dynamics · Creep · Residual deformation · Rail irregularity · Karhunen–Loeve expansion · New point estimate method

✉ Wangbao Zhou  
zhouwangbao@163.com

- <sup>1</sup> School of Civil Engineering, Central South University, Changsha, Hunan, China
- <sup>2</sup> Hunan International Scientific and Technological Innovation Cooperation Base of Advanced Construction and Maintenance Technology of Highway, Changsha University of Science & Technology, Changsha 410114, Hunan, China
- <sup>3</sup> State Key Laboratory of Hydraulic Engineering Simulation and Safety, Tianjin University, Tianjin, China
- <sup>4</sup> Chongqing Key Laboratory of Earthquake Resistance and Disaster Prevention of Engineering Structures, Chongqing University, Chongqing, China
- <sup>5</sup> Engineering Research Center of Ministry of Education for Highway Construction and Maintenance Equipment and Technology, Changan University, Xi'an, China
- <sup>6</sup> Hubei Provincial Engineering Research Center of Slope Habitat Construction Technique Using Cement Based Materials, Three Gorges University, Yichang, China

## 1 Introduction

With the continuous increase of train speed, various problems of train-bridge coupling effects gradually attracted the attention of the engineering community, and many researchers have carried out a lot of research on related issues [1–4]. The deformation of bridge is closely related to the deformation of track [5–7]. The deformation of the bridge is mainly caused by the creep of the bridge, the earthquake action, the settlement of the pier and other reasons, and then the bridge deformation directly affects the safety and comfort of driving by changing the track deformation under the influence of the above reasons [8, 9].

As we all know, seismic design is one of the most important design contents in bridge design. Most of the literatures [10–13] studied the response of the vehicle-bridge coupling system in earthquake. Wang et al. [14] showed that the influence of the lateral seismic component on the wheel derailment coefficient is greater than the vertical seismic component, and Xia et al. [15] and Zhang

et al. [16] studied train-bridge system subjected to non-uniform seismic excitations. However, after the bridge structure is subjected to a relatively large earthquake, there will be a certain degree of residual deformation [17–20], which directly leads to the deformation of the track, affecting the roughness of the track and then affecting the driving safety after the earthquake. A nonlinear numerical analytical model with multiple degrees of freedom was established to study the cumulative residual deformation of high-speed railway bridge piers under multiple earthquakes [21], but the residual deformation of the structure corresponding to the deformation of the track was not considered. Lai et al. [22] presented an analytical method of track geometry state of high-speed railway bridge under different lateral deformations, which can be conveniently obtained by the lateral displacement of bridge structure caused by external forces.

In the above literature, although the bridge deformation model and the mapping relationship between bridge deformation and track deformation have been established, the vehicle–bridge coupling problem on the deformed track under the influence of earthquake has not been studied. However, the discussion of this problem has important guiding significance for railway transportation after earthquake. At the same time, considering that most high-speed railway bridges are prestressed concrete structures, this type of structure will shrink and creep over time [23], which will cause the rise and fall of the arch of the bridge [24, 25]. Yang et al. [26] showed that the inhomogeneity of periodic creep had a significant excitation effect on both the natural and forced vibration of the vehicle, which would lead to a severe impact on the beam end of the vehicle body, thus significantly increasing the acceleration and contact force of the vehicle body.

Wen et al. [27] showed that the train parameters including load reduction rate, vertical acceleration and vertical Sperling index with temperature and creep effects were significantly different from the train parameters without these effects, indicating that creep has a greater impact on running safety. Although the influence of bridge creep on track deformation and traffic response has been studied in the literature, the comprehensive influence of vehicle–bridge coupling combined with multiple factors of track irregularity corresponding to random initial track irregularity, structural creep and post-earthquake structural residual deformation has not been considered. At the present stage, the problems of vehicle–bridge coupling need to consider the randomness of vehicle-bridge coupling vibration. The traditional deterministic model cannot satisfy the representativeness of the results due to too few excitation samples. The application of randomness can improve the representativeness of the conclusion [28]. Commonly used methods for studying randomness mainly

include MCS [29], PEM [30, 31] and PDEM [32]. Compared with the former two methods, multi-coupling excitation, such as track irregularity excitation, random vehicle load and random structural parameters, can be input into the vehicle-to-bridge coupling model established through PDEM, which greatly improves the computational efficiency [33]. Xu et al. [34] applied a probability density evolution method to solve the relationship between random track irregularity and system response, which has been turned out to be fairly effective [35, 36]. Liu [37] proposed a point estimation method (NPEM) based on adaptive dimension decomposition, which is simple to implement and highly efficient. Literatures [38–40] all used this method to solve special problems. Liu [41] analysed the influence of multiple random parameters, including random track irregularity and structural parameters, on the vehicle-axle system by combining Karhunen–Loeve expansion (KLE) and this method, and compared with MCS. It is found that the accuracy and efficiency are very high. This paper also uses this method to analyse the stochastic process.

In order to study the comprehensive effect of residual deformation and structural creep caused by earthquake on the response of vehicle and bridge system, a three-dimensional vehicle–bridge coupling model is established based on the randomness of initial track irregularity and the influence of comprehensive working conditions on track irregularity. KLE is used to reduce the dimension of initial track irregularity. The random process of the vehicle–bridge coupling system is analysed by using NPEM, and the effects of different ground motion amplitudes and different train speeds on the system response are studied.

## 2 Model and Method

### 2.1 Bridge and Track Models

As shown in Fig. 1, the main body of the bridge is composed of prestressed box girder and prestressed pier, and the track is composed of rail, track plate and base plate. In the model, the rail, beam and pier are all modelled using Bernoulli–Euler beams, and the mass and mass moment of inertia of the foundation on the bridge are included in the beam. The track plate and the base plate are thin plates. In addition, based on the finite element method, the rail, beam and pier are transformed into a series of spatial beam elements, and the track plate and base plate are transformed into plane plate elements. It is easy to know that the longitudinal, transverse and vertical elastic and damping characteristics between each of structure divisions can be simulated with discrete or continuous springs and dampers, the coefficient of which can be obtained from Fig. 1. In

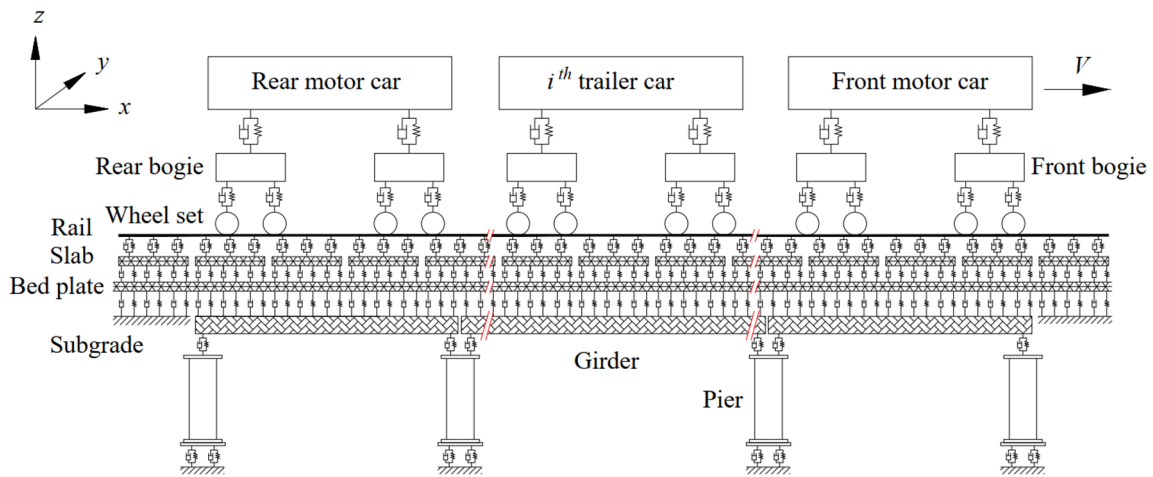


Fig. 1 Train-Track -Bridge Mode

addition, each beam element has two nodes, and each node has six degrees of freedom. Each plate element has four nodes, and each node has three degrees of freedom.

### 2.2 Train Model

As shown in Fig. 2, it is assumed that the car body, bogie and wheelset are rigid bodies. The connections between the car body and the bogie, and between the bogie and the wheelset (spring, buffer) are linear. Meanwhile, it is assumed that the wheelset is always closely attached to the rail throughout the whole process, that is, derailment will not occur. In this paper, the degrees of freedom of each car are shown in Table 1.

According to Ref. [42], the total mass matrix  $M_v$ , the total stiffness  $K_v$  and the total damping matrix  $C_v$  of the whole train can be deduced according to the energy principle.

Considering that a complete train should contain power cars at the front and rear ends and non-power cars in the middle, the total mass matrix  $M_v$  is expressed as follows:

$$M_{vv} = \text{diag}[M_{Jv1} M_{v1} \dots M_{vNv} M_{Jv2}], \tag{1}$$

where the ones with subscripts containing 'J' denote the power carriages, the others denote the non-power carriages,  $N_v$  denotes the total number of non-power carriages, and the submatrix  $M_{vi}$  denotes the mass matrix of each carriage, which takes the following form:

$$M_{vi} = \text{diag}[M_{ci} M_{t2i} M_{w1i} M_{w2i} M_{w3i} M_{w4i}], \tag{2}$$

where,  $M_{ci}$ ,  $M_{tji}$  and  $M_{wji}$  denote the mass matrix of the car-body, the  $j$ th bogie and the  $j$ th wheelset of the  $i$ th train, which takes the following form:

$$M_{ci} = \text{diag}[m_{ci} \ m_{ci} \ m_{ci} \ J_{cxi} \ J_{cyi} \ J_{czi}] \tag{3}$$

$$M_{tji} = \text{diag}[m_{ti} \ m_{ti} \ m_{ti} \ J_{txi} \ J_{tyi} \ J_{tzi}] \tag{4}$$

$$M_{wji} = \text{diag}[m_{wi} \ m_{wi} \ J_{wxi} \ J_{wzi}], \tag{5}$$

where  $m_{ci}$ ,  $m_{ti}$  and  $m_{wi}$  denote the mass of car body, bogie and wheelset.  $J_{cji}$ ,  $J_{tji}$  and  $J_{wji}$ , respectively, denote the moment of inertia of the car body, bogie and wheelset, which, respectively, represent the moment of inertia about the longitudinal, transverse and vertical axes when the subscript  $j$  is  $x$ ,  $y$  or  $z$ . The form of the mass matrix of the power car is the same as that of the non-power car, obtained by adding "J" before the subscript of these letters.

Respectively, considering that the train carriages are divided into power carriages and non-power carriages, the total stiffness matrix  $K_v$  of the train takes the following form:

$$K_{vv} = \text{diag}[K_{Jv1} K_{v1} \dots K_{vNv} K_{Jv2}], \tag{6}$$

where the one with subscript 'J' denotes power cars, and the others denote non-power cars;  $K_{vi}$  denotes the stiffness matrix of the  $i$ th carriage, which can be expressed as

$$K_{vi} = \begin{bmatrix} K_{ci} & K_{ct1i} & K_{ct2i} & 0 & 0 & 0 & 0 \\ & K_{t1i} & 0 & K_{t1w1} & K_{t1w2i} & 0 & 0 \\ & & K_{t2i} & 0 & 0 & K_{t2w3i} & K_{t2w4i} \\ & & & K_{w1i} & 0 & 0 & 0 \\ & & & & K_{w2i} & 0 & 0 \\ & \text{syms} & & & & K_{w3i} & 0 \\ & & & & & & K_{w4i} \end{bmatrix}. \tag{7}$$

The submatrix  $K_{ci}$  is expressed as

$$K_{ci} = 4 \begin{bmatrix} k_{2x} & 0 & 0 & 0 & -h_1 k_{2x} & 0 \\ & k_{2y} & 0 & h_1 k_{2y} & 0 & 0 \\ & & k_{2z} & 0 & 0 & 0 \\ & & & b_1^2 k_{2z} + h_1^2 k_{2y} & 0 & 0 \\ \text{syms} & & & & h_1^2 k_{2x} + L_c^2 k_{2z} & 0 \\ & & & & 0 & b_3^2 k_{2x} + L_c^2 k_{2y} \end{bmatrix}. \quad (8)$$

The submatrix  $K_{tji}$  is expressed as

$$K_{tji} = 2 \begin{bmatrix} 2k_{1x} + k_{2x} & 0 & 0 & 0 & -2h_3 k_{1x} - h_2 k_{2x} & 0 \\ & 2k_{1y} + k_{2y} & 0 & 2h_3 k_{1y} & 0 & 0 \\ & & 2k_{1z} + k_{2z} & 0 & 0 & 0 \\ & & & \begin{pmatrix} b_1^2 k_{2z} + 2b_2^2 k_{1z} \\ +h_2^2 k_{2y} + 2h_3^2 k_{1y} \end{pmatrix} & 0 & 0 \\ \text{syms} & & & 0 & \begin{pmatrix} h_2^2 k_{2x} + 2h_3^2 k_{1x} \\ +2L_t^2 k_{1z} \end{pmatrix} & 0 \\ & & & & & \begin{pmatrix} b_3^2 k_{2x} + 2b_4^2 k_{1x} \\ +2L_t^2 k_{1y} \end{pmatrix} \end{bmatrix}. \quad (9)$$

The submatrix  $K_{wji}$  is expressed as

$$K_{wji} = 2 \begin{bmatrix} k_{1x} & & & \\ & k_{1y} & & \\ & & b_0^2 k_{1z} & \\ \text{syms} & & & b_4^2 k_{1x} \end{bmatrix}. \quad (10)$$

The submatrix  $K_{ctji}$  is expressed as

$$K_{ctji} = -2 \begin{bmatrix} k_{2x} & 0 & 0 & 0 & h_1 k_{2x} & 0 \\ 0 & k_{2y} & 0 & -h_2 k_{2y} & 0 & 0 \\ 0 & 0 & k_{2z} & 0 & 0 & 0 \\ 0 & h_1 k_{2y} & 0 & b_1^2 k_{2z} - h_1 h_2 k_{2y} & 0 & 0 \\ -h_1 k_{2x} & 0 & (-1)^j L_c k_{2z} & 0 & -h_1 h_2 k_{2x} & 0 \\ 0 & (-1)^{j+1} L_c k_{2y} & 0 & (-1)^j h_2 L_c k_{2y} & 0 & b_3^2 k_{2x} \end{bmatrix}. \quad (11)$$

The submatrix  $K_{tjwki}$  is expressed as

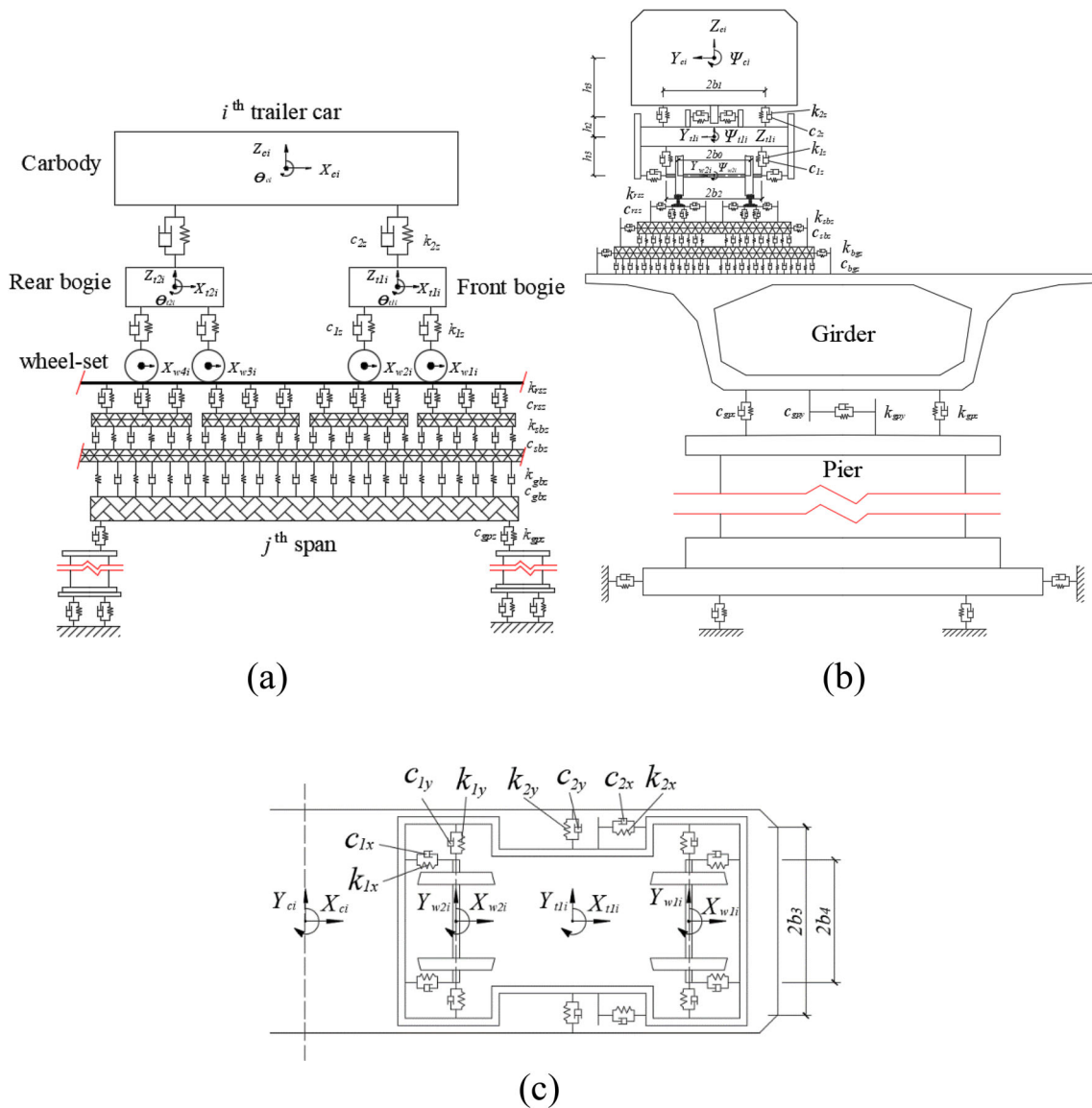


**Fig. 2** Three-dimensional model for train–slab track–bridge interaction system: **a** frontal view, **b** *j*th trailer car moving on *j*th span girder, **c** left side view, and **d** top view (without bridge)

$$K_{ijwki} = -2 \begin{bmatrix} k_{1x} & 0 & 0 & 0 \\ 0 & k_{1y} & 0 & 0 \\ 0 & 0 & 0 & 0 \\ 0 & h & (-1)^{k+1} b_0 b_2 k_{1z} & 0 \\ -h_3 k_{1x} & 0 & 0 & 0 \\ 0 & (-1)^k L_1 k_{1y} & 0 & b_4^2 k_{1x} \end{bmatrix} \quad (12)$$

The damping matrix  $C_{vv}$  of the train model is in the same form as the stiffness matrix  $K_{vv}$ , which can be obtained by replacing  $k$  of the latter with  $c$  directly.

### 2.3 Wheel–Rail Interaction

In this paper, trace method is used to calculate the wheel–rail spatial contact relationship. As shown in Fig. 3, its wheel–rail contact point  $O_R$  coordinates in the absolute coordinate system and takes form as [43], as shown in Fig. 3.

**Table 1** Degrees of freedom of train

	Longitudinal	Lateral	Vertical	Roll	Pitch	Yaw
Car-body	$X_c$	$Y_c$	$Z_c$	$\theta_c$	$\varphi_c$	$\psi_c$
Front bogie	$X_{r1}$	$Y_{r1}$	$Z_{r1}$	$\theta_{r1}$	$\varphi_{r1}$	$\psi_{r1}$
Rear bogie	$X_{r2}$	$Y_{r2}$	$Z_{r2}$	$\theta_{r2}$	$\varphi_{r2}$	$\psi_{r2}$
First wheel-set	$X_{w1}$	$Y_{w1}$	–	$\theta_{w1}$	–	$\psi_{w1}$
Second wheel-set	$X_{w2}$	$Y_{w2}$	–	$\theta_{w2}$	–	$\psi_{w2}$
Third wheel-set	$X_{w3}$	$Y_{w3}$	–	$\theta_{w3}$	–	$\psi_{w3}$
Fourth wheel-set	$X_{w4}$	$Y_{w4}$	–	$\theta_{w4}$	–	$\psi_{w4}$

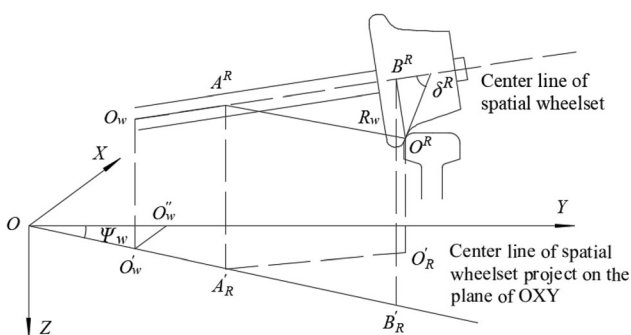


**Fig. 3** Wheel-rail geometric contact

$$\begin{cases} x_{O^R} = x_B^R + l_x R_w^R \tan \delta^R \\ y_{O^R} = y_B^R - \frac{R_w^R}{1 - l_x^2} \left( l_x^2 l_y^2 \tan \delta^R + l_z \sqrt{1 - l_x(1 + \tan^2 \delta^R)} \right) \\ z_{O^R} = z_B^R - \frac{R_w^R}{1 - l_x^2} \left( l_x^2 l_z^2 \tan \delta^R - l_y \sqrt{1 - l_x(1 + \tan^2 \delta^R)} \right) \end{cases} \quad (13)$$

$$\begin{cases} l_x = -\cos \phi_w \sin \psi_w \\ l_y = \cos \phi_w \cos \psi_w \\ l_z = \sin \phi_w \end{cases} \quad (14)$$

$$\begin{cases} x_B^R = d_w^R l_x \\ y_B^R = d_w^R l_y + Y_w \\ z_B^R = d_w^R l_z \end{cases} \quad (15)$$

where the specific meaning of the letters in the picture can be referred to Ref. [43].

At present, the solution of wheel-rail normal force is generally based on the *Hertz* nonlinear elastic contact theory [44]. Although the residual deformation caused by the seismic plastic deformation was taken into account in the irregularity of the track, the model was built after the earthquake. It was assumed that the rail remained elastic throughout the whole process, and the stiffness degradation

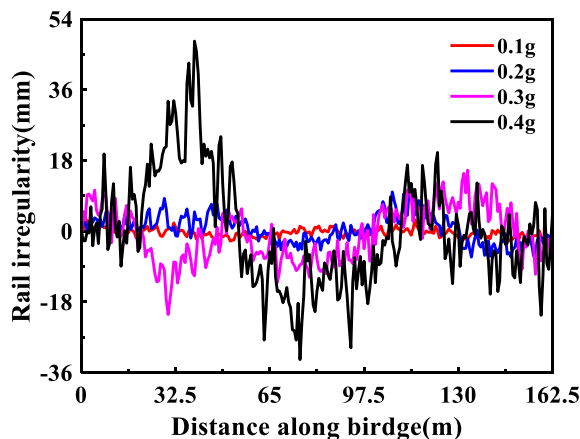


**Fig. 4** Rail irregularity caused by residual structural deformation

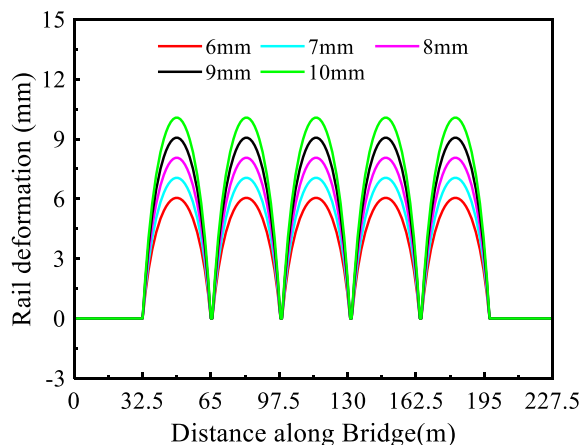


**Fig. 5** Irregularity of the rail for different attitudes of creep

was not considered, so *Hertz* elastic contact theory could still be used. By the way, although the model is set after the earthquake and the structure has undergone plastic deformation, the *Hertz* elastic contact theory can still be used if the rail remains elastic throughout the whole process and the stiffness degradation is not taken into account. The normal compression can be found in Ref. [41].

### 2.4 Seismic-Induced Track Irregularity

Lai et al. [45] established the finite element model with ANSYS program and verified the reliability of the model with the results of shaking table test. The track

**Table 2** Parameters of orbital irregularity spectrum

$\Omega_c$ /(rad/m)	$\Omega_r$ /(rad/m)	$A_a$ (m <sup>2</sup> · rad/m)	$A_v$ (m <sup>2</sup> · rad/m)
0.8246	0.0206	$2.119 \times 10^{-7}$	$4.032 \times 10^{-7}$



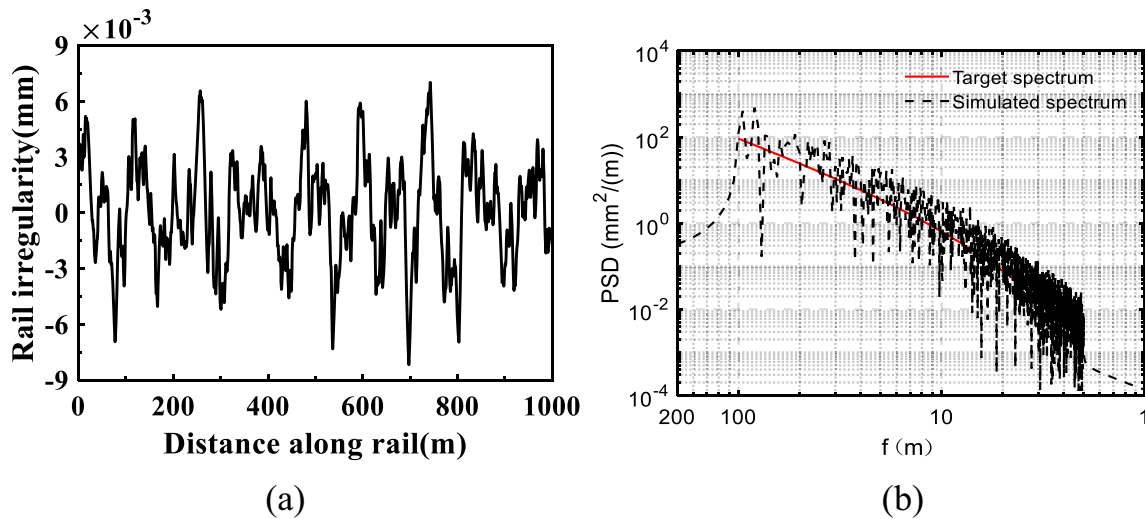


Fig. 6 a Primary track irregularity along rail on vertical rail profile. b The PSD of primary track irregularity along rail on vertical rail profile

deformations at the seismic conditions of the ground motion acceleration amplitude of 0.1 g, 0.2 g, 0.3 g and 0.4 g are obtained, as shown in Fig. 4. In this work, the data will be directly applied into the track irregularity.

### 2.5 Bridge-Creep-Induced Track Irregularity

In prestressed concrete girder bridges, concrete creep often leads to excessive deflection of the bridge and indirectly leads to vertical deformation of the rail of the track [24]. Thus, the creep is not smooth and has a great impact on running safety and comfort, so the creep of the girder bridge cannot be ignored [27].

Xiang et al. [46] established the mapping relationship between track deformation and bridge creep amplitude. Based on this method and results, the track deformation under different creep amplitude of bridge is directly obtained in this paper, as shown in Fig. 5.

### 2.6 Simulation of Initial Track Irregularity

Before the track is affected by earthquake, there is an original track irregularity, which is a random process. In this paper, KLE will be applied on multiple samples to investigate the randomness effect of initial track irregularity.

#### 2.6.1 Simulate Method of Track Irregularity

The initial sample can be generated by multiple methods, including white noise filtering method, secondary filtering

method, trigonometric series method and inverse Fourier inverse transformation method. In this work, trigonometric series method [47] is applied to generate the initial track irregularity by the German low-disturbance power spectral density (PSD).

German low interference orbit irregularity spectrum can be expressed as

$$\begin{cases} S_v(\Omega) = \frac{A_v \Omega_c^2}{(\Omega^2 + \Omega_r^2)(\Omega^2 + \Omega_c^2)}, \\ S_a(\Omega) = \frac{A_a \Omega_c^2}{(\Omega^2 + \Omega_r^2)(\Omega^2 + \Omega_c^2)} \end{cases}, \quad (16)$$

where  $S_v(\Omega)$  and  $S_a(\Omega)$  ( $m^2/(\text{rad}/m)$ ) denote the power spectral density of high and low orbit irregularity;  $\Omega$  denotes the spatial frequency of orbital irregularity ( $\text{rad}/m$ );  $\Omega_c$  and  $\Omega_r$  denote the truncation frequency ( $\text{rad}/m$ );  $A_a$  and  $A_v$  denote the roughness constant ( $m^2 \cdot \text{rad}/m$ ). The value of parameters can be found in Table 2.

Sample Generation Formula of vertical track irregularity can be expressed as

$$\tilde{z}_R(x) = \sqrt{2} \sum_{i=1}^n \sqrt{S_v(\Omega_i) \Delta\Omega} \cos(\Omega_i x + \phi_i) \quad (17)$$

$$\begin{cases} \Delta\Omega = (\Omega_n - \Omega_1)/n \\ \Omega_i = \Omega_1 + \Delta\Omega(i - 1) \quad (i = 1, 2, \dots, n) \end{cases}, \quad (18)$$

where  $\Omega_1 = 0 \text{ rad}/m$  and  $\Omega_n = 3 \text{ rad}/m$ .

The sample generation formula of track alignment irregularity is similar to the one of vertical irregularity. The samples are shown in Fig. 6a. The PSD of samples of track

irregularity is very close to the target spectrum, which denotes that the samples can be used for simulating the track irregularity. The simulated spectrum is similar to the target spectrum as shown in Fig. 6b, providing that the examples can be used to numerical analysis. The generation process and inspection result of horizon track irregularity are the same as those of the vertical ones.

### 2.6.2 Karhunen–Loeve Expansion (KLE)

KLE expansion is a method for representing random processes and is useful for random signal processing. The realization process is to compress the original data and obtain the expression with sufficient probability information of the original data by using fewer random variable dimensions.

It is assumed that  $u(x, \theta)$  is the Gaussian random distribution process,  $x$  and  $\theta$  are the position variable and parameter variable of the random process. Correspondingly,  $\bar{u}(x)$  is the mean value of  $u(x, \theta)$ . It is the covariance function of a random process. According to Mercer theory, the covariance function can be expressed as

$$C(x_1, x_2) = \sum_{n=1}^{\infty} \lambda_n \varphi_n(x_1) \varphi_n(x_2), \tag{19}$$

where  $\lambda_n$  and  $\varphi_n$  are the eigenvalues and eigenvectors of  $C(x_1, x_2)$ , and the above equation can be solved using the following equation:

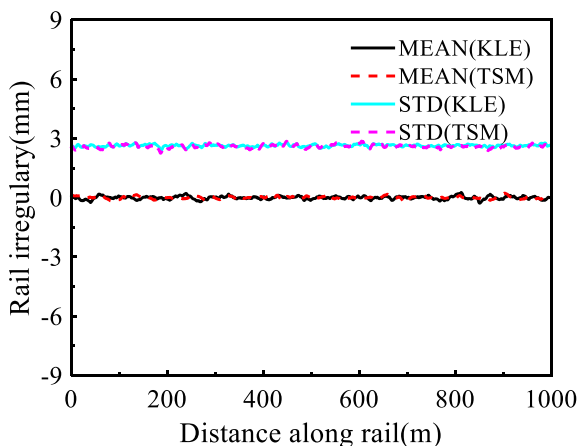


Fig. 7 Comparison of rail irregularity between KLE and TSM on vertical rail profile

$$\int_D C(x_1, x_2) \varphi_n(x_1) dx = \lambda_n \varphi_n(x_2). \tag{20}$$

The eigenvector meets orthogonality, which is described as

$$\int_D \varphi_n(x_1) \varphi_m(x_2) dx = \delta_{nm}, \tag{21}$$

where  $\delta_{nm}$  is the Kronecker function, which is described as

$$\delta_{nm} = \begin{cases} 1 & n = m \\ 0 & n \neq m \end{cases}. \tag{22}$$

Therefore, stochastic process  $u(x, \theta)$  can be obtained by

$$u(x, \theta) = \bar{u}(x, \theta) + \tilde{u}(x, \theta) = \bar{u}(x, \theta) + \sum_{n=1}^{\infty} \xi_n(\theta) \sqrt{\lambda_n} \varphi_n, \tag{23}$$

where  $\xi(\theta)$  is a set of unrelated random variables, which can be obtained by

$$\xi(\theta) = \frac{1}{\sqrt{\lambda_n}} \int_D \tilde{u}(x, \theta) \varphi_n(x) dx. \tag{24}$$

In practical application, it is only necessary to extract the first M eigenvectors and the corresponding eigenvalue to achieve data compression and reduce the amount of calculation. The modified stochastic process takes the form of

$$u(x, \theta) = \bar{u}(x, \theta) + \sum_{n=1}^M \xi_n(\theta) \sqrt{\lambda_n} \varphi_n, \tag{25}$$

where M determines the accuracy of data compression.

In this paper, it is assumed that the initial track irregularity is a one-dimensional stationary random process, and the vertical rail irregularity and the lateral one are unrelated. For each total length of artificial rail irregularity, the work has been done that a set of variable point have been taken at intervals of  $\Delta x$  along the longitudinal direction, while each sample has  $(L/\Delta x + 1)$  points.

Sufficient samples are obtained through the previous method of artificially generating rail irregularities. Assuming M samples are obtained, the total sample is  $R(x, \theta) = \{r_1(x, \theta) \ r_2(x, \theta) \ \dots \ r_n(x, \theta)\}$ , and any sample vector  $r_i(x, \theta)$  is the vector sample of  $n \times 1$ , while  $n = L/\Delta x + 1$ .

The corresponding covariance formula  $\Gamma_{R,R}$  is as follows





**Table 4** Parameters of train

Parameters	Unit	Tractor/Trailer
$m_c$ (mass of car-body)	kg	$4.8 \times 10^4 / 4.4 \times 10^4$
$J_{cx}$ (roll mass moment of car-body)	kg·m <sup>2</sup>	$1.15 \times 10^5 / 1.00 \times 10^5$
$J_{cy}$ (pitch mass moment of car-body)	kg·m <sup>2</sup>	$2.7 \times 10^6 / 2.7 \times 10^6$
$J_{cz}$ (yaw mass moment of car-body)	kg·m <sup>2</sup>	$2.7 \times 10^6 / 2.7 \times 10^6$
$M_t$ (Mass of the bogie)	kg	3200/2400
$J_{tx}$ (roll mass moment of the bogie)	kg·m <sup>2</sup>	3200/2400
$J_{ty}$ (pitch mass moment of the bogie)	kg·m <sup>2</sup>	6800/6800
$J_{tz}$ (yaw mass moment of the bogie)	kg·m <sup>2</sup>	7200/7200
$M_w$ (Mass of the wheel-set)	kg	2400/2400
$J_{wx}$ (roll mass moment of the wheel-set)	kg·m <sup>2</sup>	1200/1200
$J_{wy}$ (pitch mass moment of the wheel-set)	kg·m <sup>2</sup>	1200/1200
$k_{1x}$ (longitudinal stiffness of the first suspension system)	kN/m	9000/15000
$k_{1y}$ (lateral stiffness of the first suspension system)	kN/m	1040/700
$k_{1z}$ (lateral stiffness of the first suspension system)	kN/m	3000/5000
$k_{2x}$ (longitudinal stiffness of the second suspension system)	kN/m	240/280
$k_{2y}$ (lateral stiffness of the second suspension system)	kN/m	400/300
$k_{2z}$ (lateral stiffness of the second suspension system)	kN/m	480/560
$c_{1x}$ (longitudinal damping of the first suspension system)	kN·s/m	50/0
$c_{1y}$ (lateral damping of the first suspension system)	kN·s/m	50/50
$c_{1z}$ (lateral damping of the first suspension system)	kN·s/m	30/30
$c_{2x}$ (longitudinal damping of the second suspension system)	kN·s/m	60/120
$c_{2y}$ (lateral damping of the second suspension system)	kN·s/m	60/60
$c_{2z}$ (lateral damping of the second suspension system)	kN·s/m	30/25
$L$ (full length of the vehicle)	m	24.775/24.775
$L_c$ (half-distance of two bogies)	m	8.6875/8.6875
$L_r$ (half-distance of two wheel-sets)	m	1.25/1.25
$b_1$ (half-span of the second vertical suspension)	m	1.0/1.0
$b_2$ (half-span of the first vertical suspension)	m	0.95/0.95
$b_3$ (half-span of the second horizontal suspension)	m	1.0/1.0
$b_4$ (half-span of the first horizontal suspension)	m	0.95/0.95
$b_0$ (half-span of the wheel)	m	0.748/0.748
$e$ (lateral distance from the wheel-set to the bridge center)	m	2.5/2.5

**Table 4** (continued)

Parameters	Unit	Tractor/Trailer
$h$ (vertical distance from the rail to the bridge center)	m	1.8/1.8
$h_1$ (height of the body above the second suspension system)	m	0.8/0.8
$h_2$ (height of the second suspension system)	m	0.30/0.30
$h_3$ (height of the bogie above the wheel-set)	m	-0.05/0.10
$R_{wo}$ (Initial rolling radius of the wheel)	m	0.46/0.46

**Table 5** Parameters of PSC bridge

Parameters	Unit	value
$P_{re}$ (Control prestressing stress)	MPa	1220
$P_{loss}$ (Loss prestressing)	MPa	120
$A_{steel}$ (Area of prestressing steel bar)	m <sup>2</sup>	0.043
$A_g$ (Area of girder)	m <sup>2</sup>	8.705
$I_{gy}$ (Moment of inertia of girder)	m <sup>4</sup>	10.811
$I_{gz}$ (Moment of inertia of girder)	m <sup>4</sup>	80.945
$\nu$ (Poisson ratio of Concrete)	–	0.3
YM (Young's modulus of concrete)	MPa	$3.45 \times 10^4$
$\rho$ (Mass density of concrete)	kg/m <sup>3</sup>	2650
$\varepsilon$ (Damping ratio of concrete)	–	3%
RH (the relative environment humidity)	–	55%
$f_{cm28}$ (compressive strength of standard cubic concrete at the age of 28 days)	MPa	52.5
$P_{re}$ (Control prestressing stress)	MPa	1220
$e$ (distance between resultant force and axis of converted section of girder)	m	1.320

carried out by the Newmark –  $\beta$  method of step-by-step integration, and the system response data can be obtained.

## 2.9 New Point Estimation Method

Jiang et al. [41] proposed that when there are multiple random variables in the system and considering that the variables may be interrelated, the application of the new point estimation method (NPEM) can obtain the system response data more efficiently than MCS, so this work adopts NPEM in the simulation of the system response.

At the time  $t$ , the mean value  $\mu(t)$  and variance  $\sigma^2(t)$  of the system time history response are expressed as

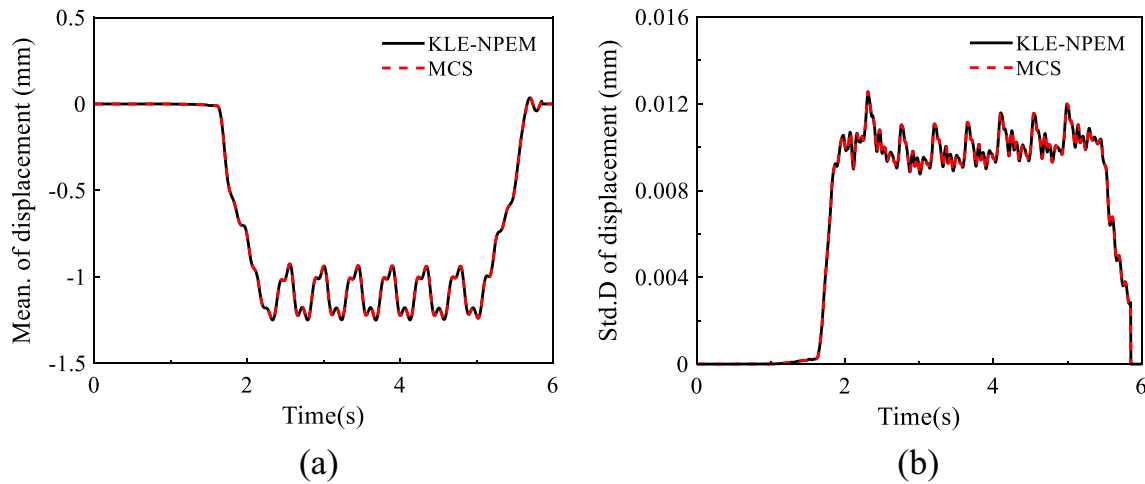


**Fig. 8** Comparison of vertical displacement of the third bridge midspan: **a** the mean value curve. **b** The standard deviation value curve

$$\mu(t) \approx \sum_{l < m} E[h(X_l, X_m, u_c, t)] - (n - 2) \sum_{k=1}^n E[h(X_k, u_c, t)] + \frac{(n - 1)(n - 2)}{2} h(u_c, t), \tag{31}$$

$$\sigma^2(t) \approx \sum_{l < m} E[h(X_l, X_m, u_c, t) - \mu(t)]^2 - (n - 2) \sum_{k=1}^n E[h(X_k, u_c, t) - \mu(t)]^2 + \frac{(n - 1)(n - 2)}{2} [h(u_c, t) - \mu(t)]^2, \tag{32}$$

where  $h(X_l, t)$  denotes the response of the system when only considering that the first variable is random and the other variables are deterministic.

$$E[(h(X_l, u_c, t) - \mu(t))^2] = \sum_{i=1}^r \frac{w_{GH,i}}{\sqrt{\pi}} (h(X_{l,i}, u_c, t) - \mu(t))^2, \tag{33}$$

$$E[(h(X_l, X_m, u_c, t) - \mu(t))^2] = \sum_{i=1}^r \frac{w_{GH,i} w_{GH,j}}{\sqrt{\pi}} (h(X_{l,i}, X_{m,j}, u_c, t) - \mu(t))^2, \tag{34}$$

where  $i$ th and  $j$ th, respectively, denote  $i$ th and  $j$ th Gauss point;  $l$ th and  $m$ th, respectively, denote  $l$ <sup>th</sup> and  $m$ <sup>th</sup> random variable

$$X_{l,i} = [x_c \ x_c \ \dots \ \sqrt{2}x_{GH,li} \ \dots \ x_c \ x_c], \tag{35}$$

where  $x_{GH,li}$  and  $w_{GH,i}$ , respectively, denote the abscissa and weight of distribution of  $l$ <sup>th</sup> variable, when  $x_c$  is the determined value of the other variables.

As shown in Table 3, the random variable is zero when the  $x_{GH,l2}$  is zero. The total random variable can be

described as  $X_{l,2} = [x_c \ x_c \ \dots \ 0 \ \dots \ x_c \ x_c]$ , with the corresponding random process result of  $h(X_{l2}, t)$ . When all random variables are considered as constants, the corresponding total constants are  $u_c = [x_c \ x_c \ \dots \ x_c \ \dots \ x_c \ x_c]$  and the corresponding random process result is  $h(u_c)$ . When the random variable is constant, it is exactly equal to the case when the variable takes the Gaussian point as the middle point. Therefore,  $h(X_{l2}, t)$  and  $h(u_c, t)$  belong to the same situation, calculation times can be greatly reduced. The total rail irregularity can be described as

$$\begin{cases} r_z(x, \theta) = r_z^{\text{creep}} \\ r_y(x, \theta) = r_y^{\text{residue}} \end{cases} \tag{36}$$

With this rail irregularity sample as the excitation, it is substituted into the vehicle and axle system, and the response  $h(X_{l2}, t)$  and  $h(u_c, t)$  can be obtained.

Taking vertical irregularity establishing as an example, the orbit irregularities of any Gaussian point corresponding to any random variable are as follows:

$$r_{li}^z(x, \theta) = r_z^{\text{creep}}(x) + \sqrt{2}x_{GH,li} \sqrt{\lambda_n} \varphi_n(x) \tag{37}$$

$$r_c^z = r_z^{\text{creep}}. \tag{38}$$

The establishment of track alignment irregularity is consistent with the establishment of vertical irregularity.

### 3 Result and Analysis of Dynamic Response

A 5-span prestressed concrete simply supported beam model is established. Each span is 32.5 m long, and the pier is 14 m high. The German ICE-3 train carriage model is adopted as the train model, and the LM model is adopted for the wheel. The structural parameters of train and bridge are shown in Tables 4 and 5. The initial track irregularity is

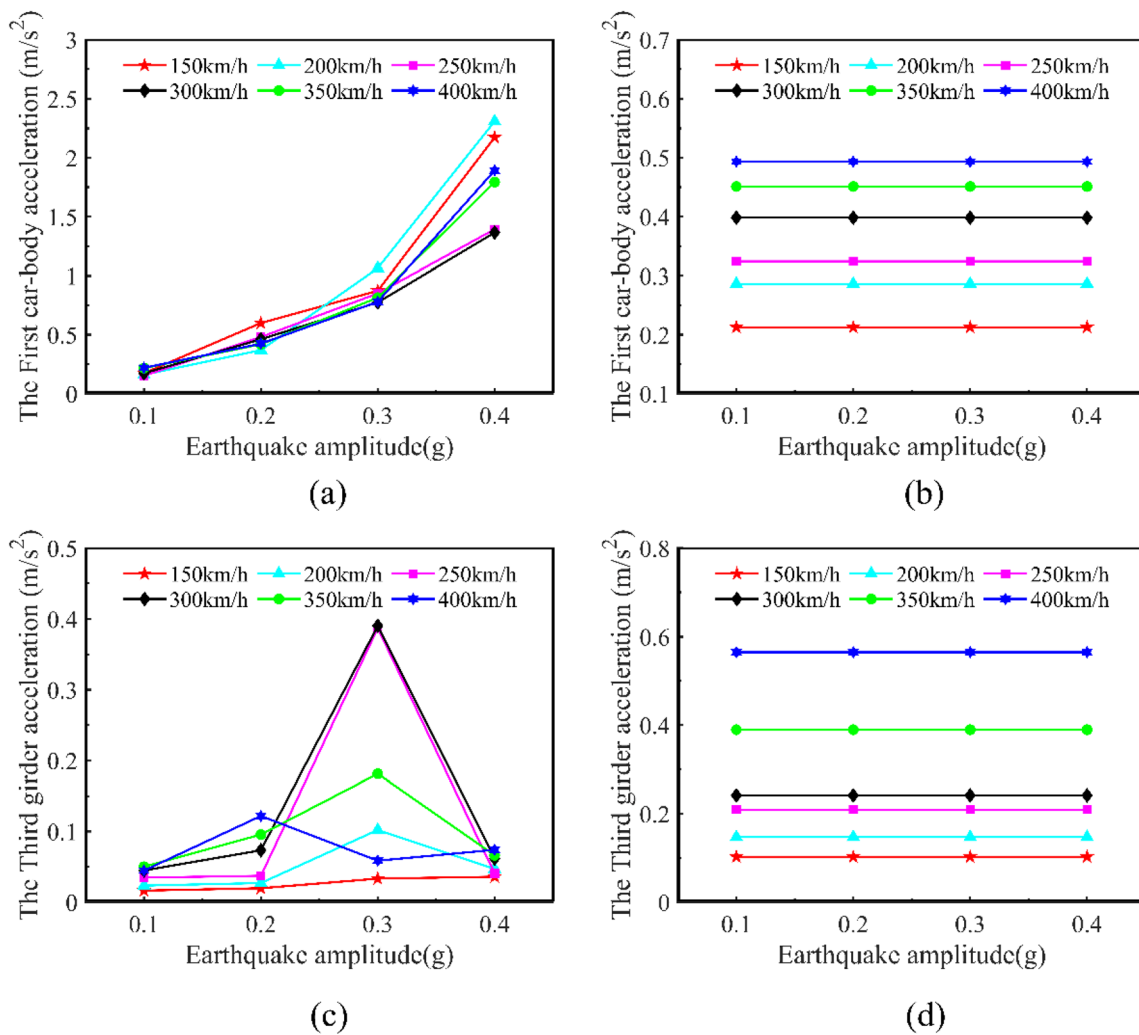


**Fig. 9** Maximum value of the lateral and the vertical acceleration of the first car-body and mid-span of the third bridge at different peaks of ground motion acceleration. **a** Lateral acceleration of car-body, **b** vertical acceleration of car-body, **c** lateral acceleration of bridge, **d** vertical acceleration of bridge

generated by the German low interference track power spectrum. KLE-NPEM is used to analyse the dynamic responses of random vibration of the vehicle-bridge coupling system, and the combined effects of residual deformation, bridge creep and initial track irregularities are also considered. For the upper and lower limits of the system response, the range of  $[\mu - 3\sigma, \mu + 3\sigma]$  is adopted, and the maximum absolute value is taken as the maximum value of system response.

### 3.1 Comparison Between MCS and NPEM

In order to verify the accuracy and efficiency of NPEM, MCS is mainly used. For the purpose of comparing MCS and KLE-NPEM, a specific case was selected with a train speed of 200 km/h, a creep amplitude of 8 mm and a

seismic acceleration of 0.2 g, and the randomness of the original track irregularity is considered.

According to the calculation, MCS conducts statistics through a large number of random initial irregularity samples of the track. In this case, the total number of calculation times of the model is 5000. KLE-NPEM conducts statistics by obtaining representative specific random samples from random samples through KLE, and intercepts the first 130 items in total. A total of 3 Gaussian points are considered for each specific random sample, so the total number of calculations is  $(130 \times 2 + 1)$ .

Figure 8 represents the mean and variance of the time-history responses of the vertical displacement and acceleration in the mid-span of the third span main girder. It also represents the process of the train passing through the bridge. When the train has not entered the bridge, the bridge is not affected, and the mean and variance of the

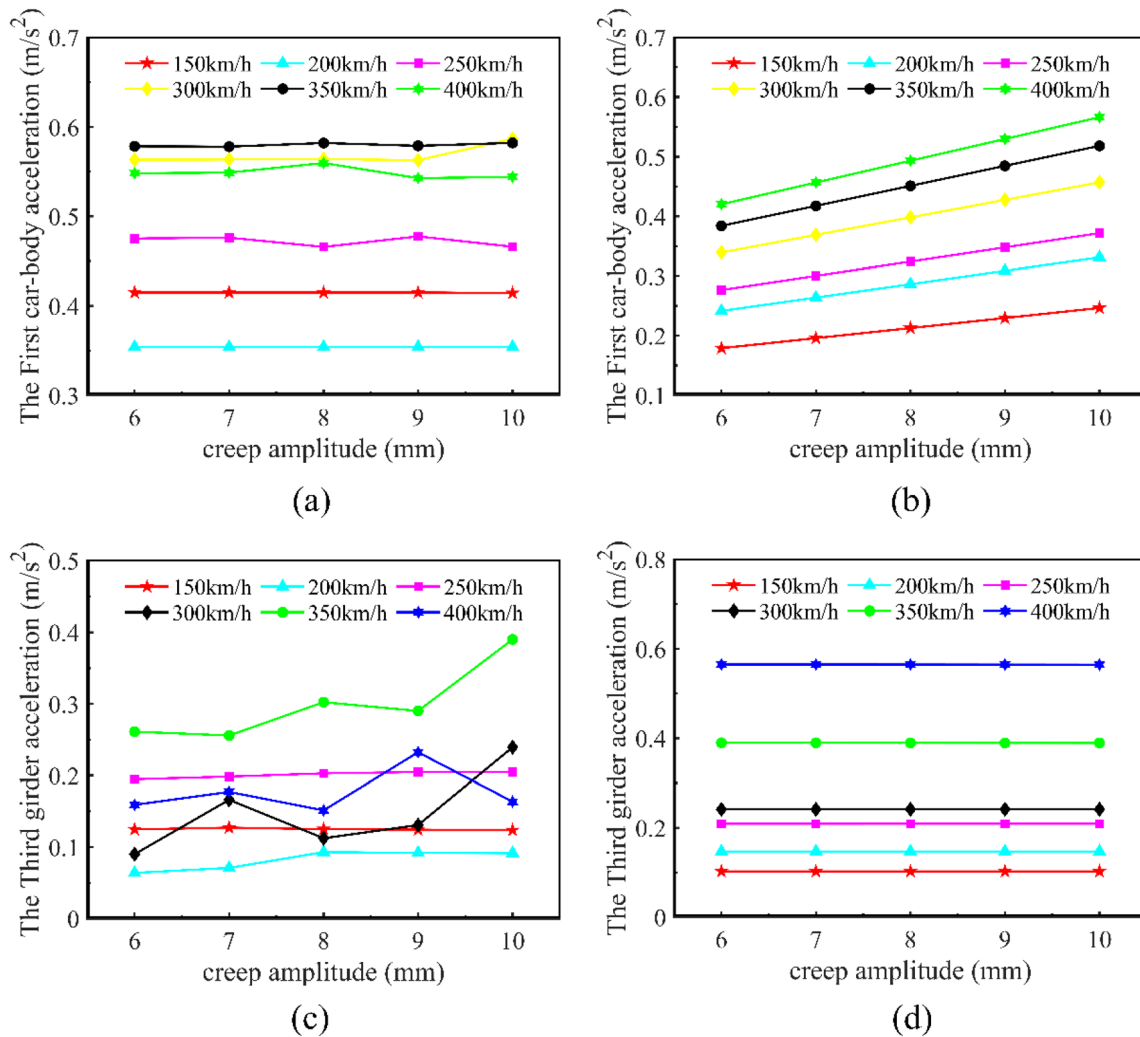


**Fig. 10** Maximum value of the lateral and vertical acceleration of the first car-body and mid-span of the third bridge at different creep amplitudes. **a** Lateral acceleration of car-body, **b** vertical acceleration of car-body, **c** lateral acceleration of bridge, **d** vertical acceleration of bridge

main girder are 0. When the train is on the bridge, the displacement starts to change, but it is relatively small. When it increases to a certain value, the change tends to be stable. The peak MEAN values calculated by NPEM and MCS were 1.2572 mm and 1.2619 mm, respectively, and the error rate was only 0.44%. The Std.D values at the same position calculated by NPEM and MCS were 0.01387 mm and 0.01415 mm, respectively, and the error rate was only 0.19%. It is clear that the mean and variance of NPEM and MCS are almost identical.

The other comparison results of dynamics response show the same conclusion, but for the limit of space of this paper, these results cannot be given here.

Based on all analysis results, the mean and variance of dynamic responses obtained by NPEM and MCS methods are highly consistent, so the NPEM method has high accuracy and reliability in analysing the random process.

At the same time, the calculation times of NPEM are much lower than that of MCS, so the former has higher computational efficiency and high feasibility. Therefore, in this work, NPEM method can be used to analyse the random process.

### 3.2 Effect of Different Peaks of Ground Motion Acceleration on Dynamic Response

Figure 9a, b shows the maximum lateral response and vertical response of the train body under different DBGA, respectively. For car body lateral response, the increase of the intensity of earthquake will directly lead to the increase of lateral response, illustrating that the residual deformation of the track after the earthquake has a great impact on the running safety of train after the main earthquake. However, it has little influence on the vertical response,

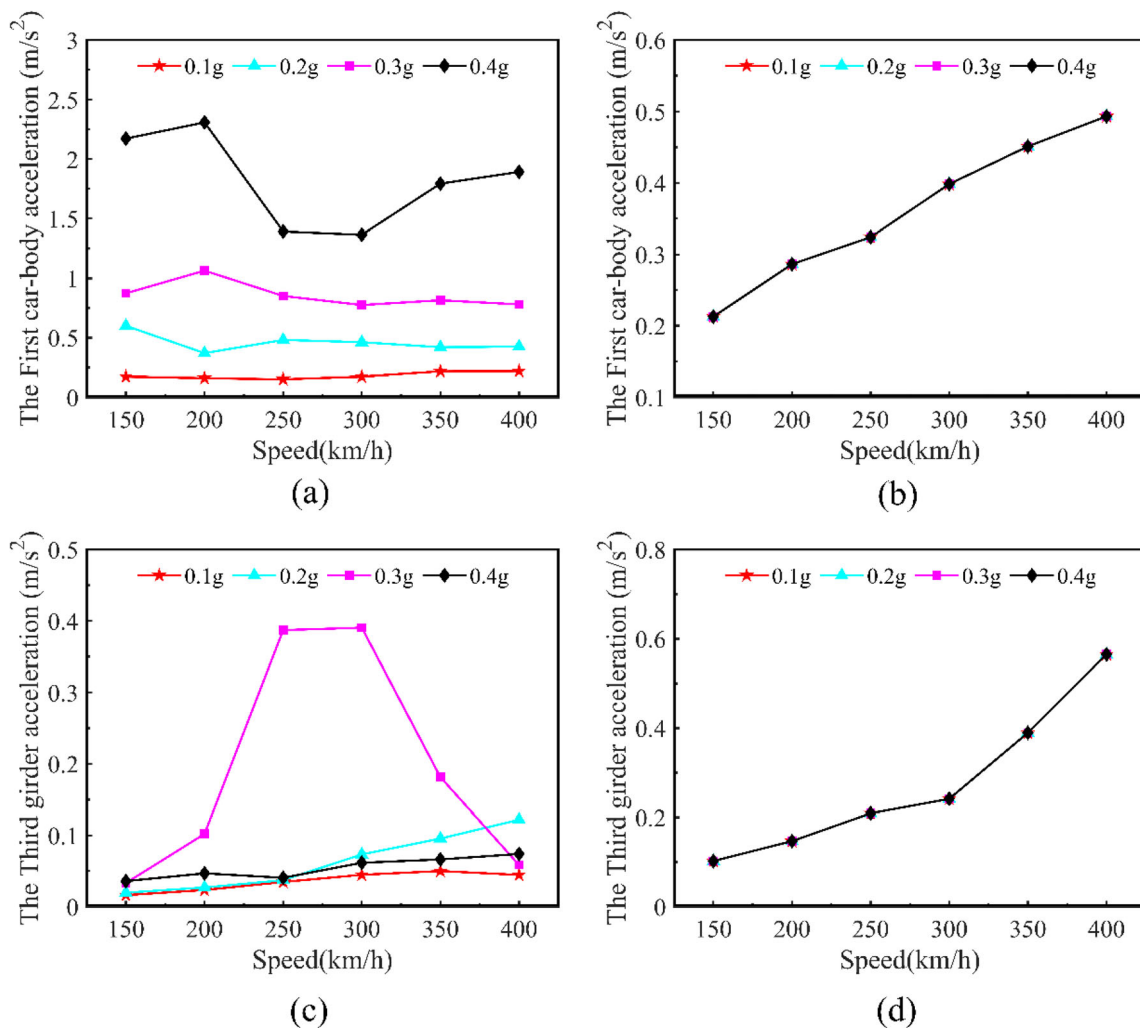


**Fig. 11** Maximum value of the lateral and vertical acceleration of the first car-body and mid-span of the third bridge at different train speeds. **a** Lateral acceleration of car-body, **b** vertical acceleration of car-body, **c** lateral acceleration of bridge, **d** vertical acceleration of bridge

which may be related to the vertical structure of train-bridge system and weak coupling between the transverse structure. In specific cases with large creep, seismic-induced rail irregularity and train speed, the acceleration of train exceeds the specified limit of  $1.3 m/s^2$ . Based on the body acceleration limit, the DBGA limit for the lateral response is 0.3 g at all speed tested.

Figure 9c, d shows the maximum lateral response and the maximum vertical response of the third span under different DBGA. In the case of different velocities, the influence of increased seismic intensity on bridge transverse response increases when DBGA increases from 0.1 to 0.3 g, but decreases after 0.3 g, indicating that the response of bridge does not change monotonously with the change of strength. However, it should depend on the actual situation that the residual deformation under different strength leads to the track irregularity. At the speed of 250–300  $km/h$ , there is a large fluctuation at 0.3 g, even exceeding the

speed of 350  $km/h$  and above, because in this case, the external load fluctuation is close to the frequency of the mid-span of the bridge. The law of vertical response is consistent with that of car, and it is not affected by the DBGA change.

### 3.3 Effect of Different Attitude of Creep on Dynamic Response

Figure 10a, b, respectively, show the maximum lateral response and maximum vertical response of the train body under different creep amplitudes. The variation of creep amplitude has a great effect on the vertical response of the vehicle body, and the effect increases with the increase of the vehicle speed. On the contrary, it has little effect on the lateral response.

Figure 10c, d, respectively, shows the maximum lateral response and maximum vertical response of the third span



under different creep amplitudes. The change of creep has a certain influence on the lateral response of the mid-span, and the change of influence is not consistent at different speeds. For example, when the speed is 250 km/h and below, it almost does not change with the creep, while there is an increasing trend at 300 km/h and above. It is interesting to find that bridge creep, a kind of vertical deformation, has less effect on the vertical response than the lateral response of mid-span acceleration. For the results, the reason is that the load caused by track irregularity and bridge creep gets closer to the natural frequencies of lateral degrees of freedom of bridges with the increase of the creep amplitude.

In summary, the development law of vertical response is consistent with the existing research results [46], but the influence of bridge creep on vertical response is very small.

### 3.4 Effect of Different Speed of Train on Dynamic Response

Figure 11a, b, respectively, show the maximum lateral response and maximum vertical response of the train body at different train speeds. The influence of change of velocity on the vertical response is much greater than that on the horizontal response. It can be clearly seen from Fig. 11a that when DBGA is 0.4 g, the change with the speed is not monotonous, and the response in the other cases is little affected by the change of the speed. It can be clearly seen in Fig. 11b that the vertical acceleration response increases monotonically with the increase of the vehicle speed.

Figure 11c, d shows the maximum lateral response of the third span of the third span at different train speeds. As it can be seen from Fig. 11c, except for the case when DBGA is 0.3 g, the acceleration will increase slowly with the increase of vehicle speed in other cases. In the case when DBGA is 0.3 g, the change of acceleration with vehicle speed is not monotonic. It will increase sharply before 250 km/h and decrease sharply after 300 km/h. There is an extreme value between 250 and 300 km/h. Resonance may occur when DBGA is 0.3 g and the speed is between 250 km/h and 300 km/h. The relationship between the vertical response and the velocity is relatively simple and monotonically increasing.

## 4 Conclusion

In this paper, the train system is simulated as a mass-damp-stiffness system, the bridge model is established by finite element method, and the dynamic equation is obtained by energy method. On this basis, a three-dimensional vehicle-bridge coupling model is constructed. The bridge creep

model and seismic bridge model are established by related software, and the additional irregularity of track is obtained. Several initial track irregularity samples obtained by trigonometric series method were used to obtain the random data through KLE. Then, the additional track irregularity was added into the random data, the accuracy of the random data was verified by probability distribution, and the random vibration response was calculated by NPEM. The results obtained by MCS simulation verify the reliability and high efficiency of NPEM. The sensitivity of the response of the vehicle body and the bridge under different ground motion acceleration amplitudes, mid-span bridge creep amplitudes and different speeds are analysed. Conclusions are obtained as follows:

- (1) First, NPEM can quickly and accurately calculate random TTBS with nonzero mean random irregularity. At the same time, the comparison between MCS and NPEM proves that NPEM is an effective method to analyse TTBCS. The average peak displacement error rate calculated by the two methods is only 0.44%.
- (2) Second, considering track irregularity of bridge creep and earthquake simultaneously, the test results of train-bridge system are more comprehensive. Although the two kinds of deformation are not in the same direction dimension, their results affect each other. For example, for bridge, the lateral seismic-induced deformation has almost no effect on the vertical response, but the vertical creep deformation has an obvious effect on the lateral response.
- (3) Third, the responses of trains and bridges have different sensitivities to the three parameters. The parameters affecting the train response from large to small are seismic peak acceleration, train speed and mid-span creep amplitude, while the parameters affecting the bridge response from large to small are vehicle speed, seismic peak acceleration and mid-span creep amplitude, which can be used as a reference for the train and the design parameters of bridges.
- (4) Finally, by considering the comprehensive situation of three kinds of track irregularities, a relatively comprehensive simulation of train running conditions after the earthquake is realized, which has a certain indicative effect on running safety after the earthquake (such as the train transportation of a large number of rescue materials after the earthquake).

**Acknowledgements** This research work was jointly supported by the National Natural Science Foundation of China (Grant No. 11972379), the Key R&D Program of Hunan Province (2020SK2060), Hunan Science Fund for Distinguished Young Scholars (2021JJ10061), CSU Innovation Driven Project (2020CX010) and Open funds of State Key

Laboratory of Hydraulic Engineering Simulation and Safety of Tianjin University, Chongqing Key Laboratory of earthquake resistance and disaster prevention of engineering structures of Chongqing University, Engineering research center of Ministry of Education for highway construction and maintenance equipment and technology of Changan University, Hubei Provincial Engineering Research Center of Slope Habitat Construction Technique Using Cement based Materials of Three Gorges University, and Hunan International Scientific and Technological Innovation Cooperation Base of Advanced Construction and Maintenance Technology of Highway of Changsha University of Science & Technology.

**Data availability** Underlying research materials related to this paper can be accessed by requesting from the corresponding author.

## Declarations

**Conflict of interest** The author(s) declared no potential conflicts of interest with respect to the research, authorship, and/or publication of this article.

## References

- Gou H et al (2021) Analytical study on high-speed railway track deformation under long-term bridge deformations and interlayer degradation. *Structures* 29:1005–1015. <https://doi.org/10.1016/j.istruc.2020.10.079>
- Xu L, Zhai W (2017) A new model for temporal-spatial stochastic analysis of vehicle-track coupled systems. *Veh Syst Dyn* 55(3):427–448. <https://doi.org/10.1080/00423114.2016.1270456>
- Ye Y et al (2021) A wheel wear prediction model of non-Hertzian wheel-rail contact considering wheelset yaw: Comparison between simulated and field test results. *Wear*. <https://doi.org/10.1016/j.wear.2021.203715>
- Zhang N, Xia H (2013) Dynamic analysis of coupled vehicle-bridge system based on inter-system iteration method. *Comput Struct* 114–115:26–34. <https://doi.org/10.1016/j.compstruc.2012.10.007>
- Chen Z, Fang H (2021) Influence of pier settlement on contact behavior between CRTS II track and bridge in high-speed railways. *Eng Struct*. <https://doi.org/10.1016/j.engstruct.2021.112007>
- Gou H et al (2018) Effect of bridge lateral deformation on track geometry of high-speed railway. *Steel Compos Struct* 29:219–229. <https://doi.org/10.12989/scs.2018.29.2.219>
- Zhou W et al (2020) Mapping relation between pier settlement and rail deformation of unit slab track system. *Structures* 27:1066–1074. <https://doi.org/10.1016/j.istruc.2020.07.023>
- Diana G et al (1995) Dynamic interaction between rail vehicles and track for high speed train. *Veh Syst Dyn* 24(sup1):15–30. <https://doi.org/10.1080/00423119508969612>
- Xu Y et al (2020) Study on the influence of lateral and local rail deformation on the train-track interaction dynamics. *Veh Syst Dyn*. <https://doi.org/10.1080/00423114.2020.1828596>
- Zhao H et al (2023) Random analysis of train-bridge coupled system under non-uniform ground motion. *Adv Struct Eng*. <https://doi.org/10.1177/13694332231175230>
- Yu J et al (2021) Study on the influence of trains on the seismic response of high-speed railway structure under lateral uncertain earthquakes. *Bull Earthq Eng*. <https://doi.org/10.1007/s10518-021-01085-1>
- Gou H et al (2017) Dynamic performance of continuous railway bridges: Numerical analyses and field tests. *Proc Inst Mech Eng Part F J Rail Rapid Transit* 232(3):936–955. <https://doi.org/10.1177/0954409717702019>
- Yang D, Pan J, Li G (2009) Non-structure-specific intensity measure parameters and characteristic period of near-fault ground motions. *Earthq Eng Struct Dyn* 38(11):1257–1280. <https://doi.org/10.1002/eqe.889>
- Wang W, Zhang Y, Ouyang H (2020) Influence of random multi-point seismic excitations on the safety performance of a train running on a long-span bridge. *Int J Struct Stabil Dyn*. <https://doi.org/10.1142/s0219455420500546>
- Xia H et al (2006) Dynamic analysis of train-bridge system subjected to non-uniform seismic excitations. *Earthq Eng Struct Dyn* 35(12):1563–1579. <https://doi.org/10.1002/eqe.594>
- Zhang N, Xia H, De Roeck G (2010) Dynamic analysis of a train-bridge system under multi-support seismic excitations. *J Mech Sci Technol* 24(11):2181–2188. <https://doi.org/10.1007/s12206-010-0812-7>
- Fahmy Mohamed FM, Wu Z, Wu G (2009) Seismic performance assessment of damage-controlled FRP-retrofitted RC bridge columns using residual deformations. *J Compos Constr* 13(6):498–513. [https://doi.org/10.1061/\(ASCE\)CC.1943-5614.0000046](https://doi.org/10.1061/(ASCE)CC.1943-5614.0000046)
- Jiang L et al (2019) Earthquake response of continuous girder bridge for high-speed railway: a shaking table test study. *Eng Struct* 180:249–263. <https://doi.org/10.1016/j.engstruct.2018.11.047>
- Jónsson MH, Bessason B, Hafliðason E (2010) Earthquake response of a base-isolated bridge subjected to strong near-fault ground motion. *Soil Dyn Earthq Eng* 30(6):447–455. <https://doi.org/10.1016/j.soildyn.2010.01.001>
- Shrestha B et al (2017) Performance-based seismic assessment of superelastic shape memory alloy-reinforced bridge piers considering residual deformations. *J Earthq Eng* 21(7):1050–1069. <https://doi.org/10.1080/13632469.2016.1190798>
- Gou H et al (2019) Modeling the cumulative residual deformation of high-speed railway bridge pier subjected to multiple earthquakes. *Earthq Struct* 17(3):317–327. <https://doi.org/10.12989/EAS.2019.17.3.317>
- Zhang XB et al (2023) Investigations on the shearing performance of ballastless CRTS II slab based on quasi-distributed optical fiber sensing. *Opt Fiber Technol* 75:103129. <https://doi.org/10.1016/j.yofte.2022.103129>
- Havlásek P et al (2021) Shrinkage-induced deformations and creep of structural concrete: 1-year measurements and numerical prediction. *Cem Concr Res*. <https://doi.org/10.1016/j.cemconres.2021.106402>
- Guo T et al (2011) Time-dependent reliability of PSC box-girder bridge considering creep, shrinkage, and corrosion. *J Bridge Eng* 16(1):29–43. [https://doi.org/10.1061/\(ASCE\)BE.1943-5592.0000135](https://doi.org/10.1061/(ASCE)BE.1943-5592.0000135)
- Yu Q, Tong T (2015) Coupled effects of static creep, cyclic creep, and damage on the long-term performance of prestressed concrete bridges: a case study based on rate-type formulation. *CONCRETE* 10:229–237. <https://doi.org/10.1061/9780784479346.027>
- Yang H et al (2014) Dynamic analysis of train-rail-bridge interaction considering concrete creep of a multi-span simply supported bridge. *Adv Struct Eng* 17(5):709–720. <https://doi.org/10.1260/1369-4332.17.5.709>
- Li WQ, Zhu Y, Li XZ (2012) Dynamic response of bridges to moving trains: a study on effects of concrete creep and temperature deformation. *Appl Mech Mater* 193–194:1179–1182. <https://doi.org/10.4028/www.scientific.net/AMM.193-194.1179>

28. Yu Z-W et al (2016) Non-stationary random vibration analysis of a 3D train–bridge system using the probability density evolution method. *J Sound Vib* 366:173–189. <https://doi.org/10.1016/j.jsv.2015.12.002>
29. Lombaert G, Conte Joel P (2012) Random vibration analysis of dynamic vehicle–bridge interaction due to road unevenness. *J Eng Mech* 138(7):816–825. [https://doi.org/10.1061/\(ASCE\)EM.1943-7889.0000386](https://doi.org/10.1061/(ASCE)EM.1943-7889.0000386)
30. Zhang J et al (2012) Non-stationary random vibration of a coupled vehicle–slab track system using a parallel algorithm based on the pseudo excitation method. *Proc Inst Mech Eng Part F J Rail Rapid Transit* 227(3):203–216. <https://doi.org/10.1177/0954409712458403>
31. Zhao H et al (2022) Seismic running safety assessment for stochastic vibration of train–bridge coupled system. *Arch Civ Mech Eng* 22(4):180. <https://doi.org/10.1007/s43452-022-00451-3>
32. Li J et al (2012) Advances of the probability density evolution method for nonlinear stochastic systems. *Probab Eng Mech* 28:132–142. <https://doi.org/10.1016/j.probengmech.2011.08.019>
33. Yu Z-W, Mao J-F (2018) A stochastic dynamic model of train-track-bridge coupled system based on probability density evolution method. *Appl Math Model* 59:205–232. <https://doi.org/10.1016/j.apm.2018.01.038>
34. Xu L, Zhai W, Gao J (2017) A probabilistic model for track random irregularities in vehicle–track coupled dynamics. *Appl Math Model* 51:145–158. <https://doi.org/10.1016/j.apm.2017.06.027>
35. Xu L, Zhai W (2017) Stochastic analysis model for vehicle–track coupled systems subject to earthquakes and track random irregularities. *J Sound Vib* 407:209–225. <https://doi.org/10.1016/j.jsv.2017.06.030>
36. Xu L, Chen Z, Zhai W (2017) An advanced vehicle–slab track interaction model considering rail random irregularities. *J Vib Control* 24(19):4592–4603. <https://doi.org/10.1177/1077546317731005>
37. Fan W et al (2016) Adaptive estimation of statistical moments of the responses of random systems. *Probab Eng Mech* 43:50–67. <https://doi.org/10.1016/j.probengmech.2015.10.005>
38. Ahmadabadi M, Poisel R (2015) Probabilistic analysis of rock slopes involving correlated non-normal variables using point estimate methods. *Rock Mech Rock Eng* 49(3):909–925. <https://doi.org/10.1007/s00603-015-0790-2>
39. Chen C et al (2015) Correlated probabilistic load flow using a point estimate method with Nataf transformation. *Int J Electric Power Energy Syst* 65:325–333. <https://doi.org/10.1016/j.ijepes.2014.10.035>
40. Xie X, Krewer U, Schenkendorf R (2018) Robust Optimization of Dynamical Systems with Correlated Random Variables using the Point Estimate Method Financial support of Promotionsprogramm “ $\mu$ -Props” by MWK Niedersachsen is gratefully acknowledged. *IFAC-PapersOnLine* 51(2):427–432. <https://doi.org/10.1016/j.ifacol.2018.03.073>
41. Jiang L et al (2019) Train-bridge system dynamics analysis with uncertain parameters based on new point estimate method. *Eng Struct*. <https://doi.org/10.1016/j.engstruct.2019.109454>
42. Zeng Z-P et al (2016) Formulation of three-dimensional equations of motion for train–slab track–bridge interaction system and its application to random vibration analysis. *Appl Math Model* 40(11–12):5891–5929. <https://doi.org/10.1016/j.apm.2016.01.020>
43. Xia H, Zhang N, Guo W (2018) Dynamic analysis of train-bridge coupling system. In: Xia H, Zhang N, Guo W (eds) *Dynamic interaction of train-bridge systems in high-speed railways: theory and applications*. Springer, Berlin Heidelberg, Berlin, pp 227–289
44. Johnson KL (2009) Contact mechanics. *Proc Inst Mech Eng* 223(J3):254
45. Zhao H et al (2023) A velocity-related running safety assessment index in seismic design for railway bridge. *Mech Syst Signal Process* 198:110305. <https://doi.org/10.1016/j.ymsp.2023.110305>
46. Xiang P et al (2021) Investigations on the influence of prestressed concrete creep on train-track-bridge system. *Constr Build Mater*. <https://doi.org/10.1016/j.conbuildmat.2021.123504>
47. Zhai W (2015) *Vehicle-track coupled dynamics*, 4th edn. Science Press, Beijing (**Springer**)

Springer Nature or its licensor (e.g. a society or other partner) holds exclusive rights to this article under a publishing agreement with the author(s) or other rightsholder(s); author self-archiving of the accepted manuscript version of this article is solely governed by the terms of such publishing agreement and applicable law.